Turk J Chem
31 (2007) , 427 – 443.

A Mechanistic Approach to Elucidate Ethanol Electro-oxidation

Niyazi Alper TAPAN
Department of Chemical Engineering, Gazi University, Ankara-TURKEY
e-mail: atapan@gazi.edu.tr

Received 08.02.2007

In order to elucidate the mechanism of ethanol oxidation, a simple cylindrical diffusion-surface reaction was developed on a platinum disk electrode. An ethanol electro-oxidation mechanism was proposed, in which electrochemical reactions proceed without adsorption of any electro-oxidation products (C2 type) on the surface. After the simulation of the proposed mechanism, it was seen that the model can explain ethanol electro-oxidation behavior without any surface CO formation. The simulation of the mechanism indicated that the formation of acetaldehyde through the oxidation of bulk ethanol is the rate determining step between 0.6 and 0.75 V vs. RHE. After 0.75 V vs. RHE, the formation of surface acetate through bulk ethanol becomes the rate determining step. According to the proposed oxidation model, around 0.7 V vs. RHE, acetaldehyde coverage becomes the major surface species, and acetate formation starts around 0.7 V vs. RHE. Surface species profiles of the proposed model show that C2 type species play an important role in ethanol electro-oxidation.

Key Words: Ethanol, electro-oxidation, mechanism, fuel cell, current.

Introduction

Today, low temperature polymer electrolyte membrane fuel cells operated by direct injection of liquid fuels are gaining importance every day because of their large application potential in portables, stationary systems, and vehicles and also because of their simplified system without any external reformer.

Liquid fuels, used in polymer electrolyte membrane fuel cells (PEMFCs) are low molecular weight alcohols (such as methanol and ethanol) exhibiting higher energy densities and better energy efficiency than gaseous fuels. Furthermore, alcohols can also be stored and transported easily. Today, short chain alcohols such as ethanol other than methanol, which is relatively toxic, are being tested for direct liquid electro-oxidation PEMFCs. Ethanol is safer and has more energy density (316.83 kcal/mol) than methanol (166.77 kcal/mol).[1] Ethanol is also environmentally friendly and can be easily produced by the fermentation of sugar containing raw materials.

In order to make ethanol an effective fuel for direct alcohol fuel cells, many research groups have studied the adsorption and oxidation of ethanol to identify reaction intermediates and products. Since ethanol is electrochemically oxidized through different pathways on different catalytic surfaces, it is more difficult to elucidate the mechanism of ethanol electro-oxidation than methanol.[2]

In this study, we developed a simple ethanol electro-oxidation model on a platinum disk electrode, performed a kinetic study for the proposed oxidation model, and determined the surface concentration distributions.

Theory and Calculations

Model

A cylindrical diffusion-surface reaction model was developed on a platinum disk electrode for the electro-oxidation of ethanol. Mass transport was included in this model in order to see the contribution of diffusion current (in z and r directions) to the total current during ethanol electro-oxidation. Our model consists of 2 layers (Figure 1):

Layer I: The electroactive species adsorb or desorb at the same time and electrochemical surface reactions take place. This layer can also be assumed to be an outer Helmholtz plane where the reactant moves close to the electrode surface and the electron is exchanged on this layer.

Layer II: Diffusion rate is equal to adsorption plus desorption rate of soluble species.

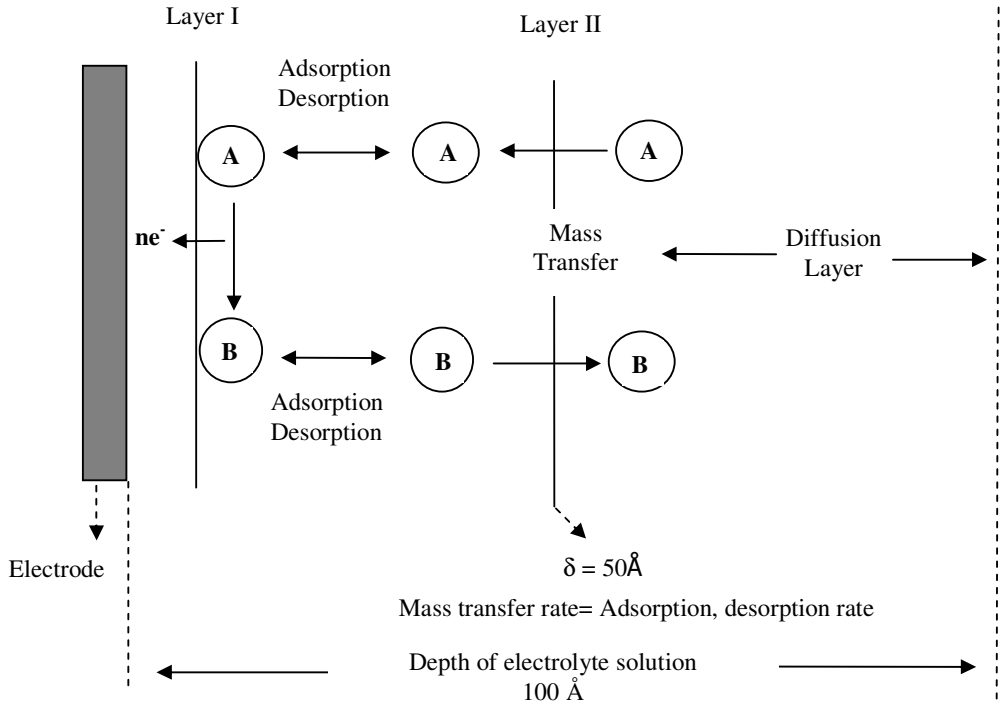

Figure 1. Representation of the anode electrode surface layer considered for the ethanol oxidation model.

In the model, the surface layer is composed of 2 layers as mentioned above and the thickness of each layer is assumed to be 50 Å (and the thickness of the surface layer is less than 100 Å).[3]

Layer II

Initially, for layer II, 3 main soluble species were considered for our diffusion model. These species are ethanol (C_2H_5OH), acetaldehyde ($CHOCH_3$), and acetic acid (CH_3COOH), which were identified by spectroelectro-

chemical and chromatographic techniques.[4−8] The diffusion of these soluble species during ethanol oxidation occurs in both z (depth of electrolyte solution) and r (radius of the disk) directions in the electrolyte solution.

Differential species material balance in the electrolyte solution is given in Eq. (1) below:

For $t > 0$, $L \geq z > \delta_o$, $r_o > r > 0$

(where δ_o, L, and r_o denote the thickness of layer II, the depth of electrolyte solution, and the radius of the disk electrode, respectively.)

$$\frac{1}{r} \cdot \frac{\partial}{\partial r} \cdot \left(D_i \cdot r \cdot \frac{\partial C_i}{\partial r} \right) + \frac{\partial}{\partial z} \cdot \left(D_i \cdot \frac{\partial C_i}{\partial z} \right) = \frac{\partial C_i}{\partial t} \tag{1}$$

Equation (1) shows that the unsteady state diffusion of soluble species takes place between layer II and the depth of electrolyte solution (semi-infinite medium). The 2-dimensional, elliptic, second-order, partial differential equation (Eq. (1)) was solved by the finite differences method.[9]

Finite differences approximation of Eq. (1) is given in Eq. (2) below:

For t → n, r → i, z → j

$$\begin{aligned} &C_i(i,j,n+1) = C_i(i,j,n).(1 - \Delta t.D_i/i/\Delta r^2 - 2.\Delta t.D_i/\Delta r^2 - 2.\Delta t.D_i/\Delta z^2) + \\ &C_i(i-1,j,n).(\Delta t.D_i/\Delta r^2) + C_i(i+1,j,n) \\ &(\Delta t.D_i/i/\Delta r^2) + C_i(i,j+1,n).(\Delta t.D_i/\Delta z^2) + C_i(i,j-1,n).(\Delta t.D_i/\Delta z^2) \end{aligned} \tag{2}$$

In order to solve Eq. (1), we need 1 initial and 3 boundary conditions given below,

Initial condition:
For t = 0, $L \geq z > \delta_o$, $r_o > r > 0$,

$C_{I,S} = 0$, where $C_{I,S}$ denotes the concentration of surface species (mol/cm^2),

$C_V = 4.47$ nmol/cm^2, where C_V denotes the surface density of vacant surface sites,

$C_{C2H5OH} = 0.5$ mol/cm^3, where C_{C2H5OH} denotes the bulk concentration of ethanol in the electrolyte,

$C_{CHOCH3} = 0$ mol/cm^3, where C_{CHOCH3} denotes the bulk concentration of acetaldehyde in the electrolyte,

$C_{CH3COOH} = 0$ mol/cm^3, where $C_{CH3COOH}$ denotes the bulk concentration of acetic acid in the electrolyte,

$C_{H2O} = 2.2$ mol/cm^3, where C_{H2O} denotes the bulk concentration of water in the electrolyte,

Boundary conditions:

Boundary condition 1,
For $t > 0$, $z = \delta_o$, $r_o > r > 0$

$$-D_i \cdot \frac{dC_i(\delta_o, r, t)}{dz} = k_{ads} \cdot C_i(\delta_o, r, t) \cdot C_V(r, t) - k_{des} \cdot C_{iS}(r, t) \tag{3}$$

Boundary condition 1 shows that at layer II diffusion flux is equal to the adsorption and desorption rate of the soluble species.

The finite difference approximation of Eq. (3) is given in Eq. (4):

$$C_i(i,1,n+1) = (C_i(i,2,n+1) - k_{des,i}.C_{is}(i,n+1).\Delta z/D_i)/(1 - k_{ads,i}(n).\Delta z/D_i.C_v(i,n+1) - k_i(n).C_v(i,n+1).\Delta z/D_i) \quad (4)$$

Boundary condition 2,
For $t > 0$, $z = L$, $r_o > r > 0$

$$\frac{dC_i}{dz} = 0 \quad (5)$$

Boundary condition 3,
For $t > 0$, $r = 0, r_o$, $L \geq z > \delta$

$$\frac{dC_i}{dr} = 0 \quad (6)$$

Boundary conditions 2 and 3 imply that the concentration of bulk species approaches a finite value at the bottom of electrolyte solution and at the center and the edge of the disk electrode.

After species material balance (Eq. (1)) was solved by finite differences approximation, diffusion current can also be evaluated in the r and z directions (Eq. (7)):

$$I_d = F.A.\sum z_i \cdot D_i.\frac{\partial C_i}{\partial r} + F.A.\sum z_i \cdot D_i.\frac{\partial C_i}{\partial z} \quad (7)$$

Finite difference approximation of Eq. (7) is given in Eqs. (8) and (9),

Diffusion current in z direction:

$$Id_Z(i,j,n+1) = F.A.\sum(D_i.(C_i(i,j+1,n+1) - C_i(i,j,n+1))/\Delta z) \quad (8)$$

Diffusion current in r direction:

$$Id_R(i,j,n+1) = F.A.\sum(D_i.(C_i(i+1,j,n+1) - C_i(i,j,n+1))/\Delta r) \quad (9)$$

The diffusion coefficients of soluble species in the electrolyte (as seen in Eqs. (1), (3), and (7)) were estimated by Stokes-Einstein equation[10,11] (Eq. (10)):

$$D_i = \frac{k_B \cdot T}{f \cdot \pi \cdot r \cdot \eta} \quad (10)$$

In Eq. (10), k_B is the Boltzmann constant (1.3807×10^{-23} J.K^{-1}); r is the radius of the solute; f is a constant, which is 6 in water; and η is the viscosity of the solvent. From Eq. (10), the diffusion coefficients of the solubles were estimated to be $\sim 10^{-9}$ m^2/s. It was clear that, in an electrolyte solution, the diffusion coefficients are ranging between 1 and 10×10^{-9} m^2/s.

Layer I

At layer I, the adsorption and desorption of the soluble species along with electrochemical surface reactions take place. The rate of change of surface species and the anodic faradaic current at layer I can be expressed as given in Eqs. (11) and (12):

For $t > 0$, $r_o \geq r \geq 0$, $z =$ layer I

$$\frac{dC_{iS}(r,t)}{dt} = k_{iads} \cdot C_{i,z=\delta}(r,t) \cdot C_v(r,t) - k_{ides} \cdot C_{i,s}(r,t) + \sum_{j=1}^{m} k_j \cdot \exp\left[\frac{(1-\gamma)\cdot n \cdot F}{R \cdot T} \cdot \left(\varepsilon(t) - \varepsilon_j^o\right)\right] \cdot C_{i,S} \quad (11)$$

$$I_f = A.\Sigma\nu_j.F.k_j.C_{js}(r,t).\exp((1-\gamma).F.(\varepsilon(t) - \varepsilon_j^o)/(R.T)) \quad (12)$$

Numerical integration of Eq. (11) was done by using Euler's method to find the surface species concentrations, $C_{i,S}$ (r,t). After that, $C_{i,S}$(r,t) was incorporated into boundary condition 1 (Eq. (3)). In Eq. (12), A, ν_j , ε, ε^o ,γ, and k_j denote disk electrode area, number of equivalence for the surface electrochemical reaction (Butler-Volmer reaction), applied potential, the equilibrium potential, symmetry number (which is assumed to be 0.5)[3], and preexponential factor, respectively.

Change in vacant surface concentration on the platinum surface was estimated by assuming that the platinum metal has a langmuirian surface (each surface species occupy one site without any interaction with each other) (Eq. (13)):

$$C_T = \sum_i C_{iS}(r,t) + C_V(r,t) \quad (13)$$

In Eq. (13) above, C_T is the active site concentration on the platinum surface, which is explained in the experimental section. If the differential of Eq. (13) with respect to time is obtained, the rate of change in vacant surface concentration (mol/cm^2) on the platinum surface can be estimated as given in Eq. (14):

$$\frac{dC_\nu(r,t)}{dt} = -\sum_{i=1}^{n} \frac{dC_{i,s}}{dt} \quad (14)$$

The rate of change in surface species is also given in Eqs. (15) through (18):

$$\frac{dC_{CHOCH3S}(r,t)}{dt} = k_1 \cdot \exp\left[\frac{(1-\gamma)\cdot 2.F}{R\cdot T} \cdot (\varepsilon(t) - \varepsilon_1^o)\right] \cdot C_{C2H5OH,z=\delta}(r,t) \cdot C_{H2OS}(r,t) - k_2 \cdot C_{CHOCH3S}(r,t) \quad (15)$$

$$\frac{dC_{H2OS}(r,t)}{dt} = k_3 \cdot C_{H2O,z=\delta}(r,t) \cdot C_v(r,t) - k_4 \cdot \exp\left[\frac{(1-\gamma)\cdot F}{R\cdot T} \cdot (\varepsilon(t) - \varepsilon_4^o)\right] \cdot C_{H2OS}(r,t) \quad (16)$$

$$\begin{aligned}\frac{dC_{OHS}(r,t)}{dt} &= k_4 \cdot \exp\left[\frac{(1-\gamma)\cdot F}{R\cdot T} \cdot (\varepsilon(t) - \varepsilon_4^o)\right] \cdot C_{H2OS}(r,t) \\ &- k_5 \cdot \exp\left[\frac{(1-\gamma)\cdot 4.F}{R\cdot T} \cdot (\varepsilon(t) - \varepsilon_5^o)\right] \cdot C_{OHS}(r,t) \cdot C_{C2H5OH,z=\delta}(r,t) \\ &- k_6 \cdot \exp\left[\frac{(1-\gamma)\cdot F}{R\cdot T} \cdot (\varepsilon(t) - \varepsilon_6^o)\right] \cdot C_{OHS}(r,t) \cdot C_{CHOCH_3,z=\delta}(r,t) \\ &- k_7 \cdot \exp\left[\frac{(1-\gamma)\cdot 2.F}{R\cdot T} \cdot (\varepsilon(t) - \varepsilon_7^o)\right] \cdot C_{OHS}(r,t) \cdot C_{CHOCH_3,z=\delta}(r,t)\end{aligned} \quad (17)$$

$$\frac{dC_{CH3COOS}(r,t)}{dt} = k_5 \cdot \exp\left[\frac{(1-\gamma)\cdot 4.F}{R\cdot T}\cdot\left(\varepsilon\left(t\right)-\varepsilon_5^o\right)\right]\cdot C_{OHS}\left(r,t\right)\cdot C_{C2H5OH,z=\delta}\left(r,t\right)$$
$$+k_7 \cdot \exp\left[\frac{(1-\gamma)\cdot 2.F}{R\cdot T}\cdot\left(\varepsilon\left(t\right)-\varepsilon_7^o\right)\right]\cdot C_{OHS}\left(r,t\right)\cdot C_{CHOCH_3,z=\delta}\left(r,t\right) \quad (18)$$

In Eqs. (15)-(18), k_1, k_4, k_5, k_6, and k_7 denote preexponential factors for Butler-Volmer reactions; k_2 and k_3 denote the desorption and adsorption rate constants for acetaldehyde and water. The rate of change in surface species was derived with respect to the surface reaction mechanism, which is discussed in the next section.

The adsorption rate constant for water, k_3, on a positive platinum electrode was approximated as in Eq. (19):[12−18]

$$k_3 = 0.0943\cdot Sinh\left(\frac{\Delta\psi}{2}\right)\cdot\exp\left[\beta\cdot\mu_w\left(-\frac{2\cdot\kappa}{\beta\cdot n\cdot e}\cdot Sinh\left(\frac{\Delta\psi}{2}\right)\right)\right]\cdot\exp\left[-2.4635\cdot\Gamma\cdot\delta\right] \quad (19)$$

In Eq. (19), $\Delta\Psi$ is $(\Psi - \Psi_{ref})$ where Ψ is the applied potential and Ψ_{ref} is the equilibrium potential given in Table 1. Γ is the Debye Hueckel screening length 100 Å, μ_w is the dipole moment of water taken as 6.2×10^{-30}, and δ is the diameter of water molecule taken as 2.8 Å.

The desorption rate constant for acetaldehyde (k_2) was defined in Eq. (20):

$$k_2 = A_{id}\cdot\exp\left[\frac{-Ed_i}{R\cdot T}\right] \quad (20)$$

In Eq. (20), Ed_i is the desorption energy and A_{id} is the frequency factor (Table 1).

Table 1. Chemical surface reaction mechanism on layer I.

Possible Non-electrochemical reactions and adsorption-desorption steps	Frequency factor, $A_{id}, (1/s)$	Adsorption Energy (kJ/mol)	E_o (V vs. RHE)	Ed(Desorption energy)
$CHOCH_3.Pt \rightarrow CHOCH_3 + Pt$	$\sim 10^{13}$[22] -			$\sim$86 kJ/mol[23]
$H_2O + Pt \rightarrow H_2O.Pt$		40.17[23,24]	0.05[19]	

Surface reaction mechanism

In order to derive the rate of change of surface species on the platinum electrode (Eqs. (15)-(18)), ethanol electro-oxidation products and by-products were investigated on the platinum surface.

According to previous studies, onset of ethanol oxidation starts at a potential of 0.3 V vs. RHE and acetaldehyde is detected at potentials of 0.35 V vs. RHE. At potentials higher than 0.55 V vs. RHE, electrochemical oxidation of water leads to a more complete oxidation of adsorbed species to acetic acid without breaking the C-C bond.[4−8]

Acetaldehyde, which is a by-product of ethanol oxidation, is an unstable molecule over Pt(III) at temperatures above room temperature and further oxidation of acetaldehyde operates in competition with acetaldehyde desorption.[20] FTIR results also show that ethanol oxidation on platinum occurs via parallel

pathways producing CO_2, acetic acid, and acetaldehyde. Although when the Pt electrode was polarized at 0.5 V vs. RHE in 1 M C_2H_5OH + 0.1M $HClO_4$ solution, it was observed that CO_2 production was much lower than acetic acid and acetaldehyde production according to the FTIR spectra.[21]

ATR (attenuated total reflection) and SEIRAS (surface enhanced infrared absorption spectroscopy) studies indicated that acetate formation happens between 0 and 1.07 V vs. RHE. Electrochemical formation of acetate requires surface hydroxyl as a source. SEIRA results indicate that acetate has the highest coverage on the platinum surface together with acetaldehyde. Since surface acetate is strongly bonded to the surface, it is difficult to oxidize it further to CO_2 and desorption is unfavorable in the potential range studied.[20] When background-corrected ethanol electro-oxidation on the platinum electrode was analyzed, an oxidation peak was detected at around 0.65 V vs. RHE. This current peak was attributed to the formation of acetate mainly. The formation of acetate was also compared with the oxidation of CO_L (linearly bonded carbon monoxide) by FTIR band intensities. Linearly adsorbed CO intensity decreases sharply around 0.3 V vs. RHE and the intensity becomes negligible around 0.5 V vs. RHE. The source of CO_L was linked to the strongly adsorbed acetaldehyde and the acetyl (Eqs. (21)-(24)):

$$C_2H_5OH + H_2O.Pt \rightarrow CHOCH_3.Pt + 2H^+ + H_2O + 2e^- \tag{21}$$
$$CHOCH_3.Pt + Pt \rightarrow Pt.CH_3 + Pt.CO + H^+ + e^- \tag{22}$$
$$CHOCH_3.Pt \rightarrow Pt.CH_3CO + H^+ + e^- \tag{23}$$
$$Pt.CH_3CO \rightarrow Pt.CH_3 + Pt.CO \tag{24}$$

In order to see the existence of oxidation currents before 0.5 V vs. RHE and current peak around 0.65 V vs. RHE, ethanol electro-oxidation experiments were performed in a 3-electrode cell environment (experimental section). No appreciable current was observed before 0.53 V vs. RHE (Figure 4 in experimental section), which was mostly attributed to the oxidation of surface carbon monoxide. Due to the negligible oxidation current before 0.53 V vs. RHE, a different mechanism (Eqs. (25)-(28)) for the platinum electrode in a 0.5 M H_2SO_4 electrolyte solution was considered and the existence of the mechanism in the potential range of concern (0-1 V vs. RHE) was investigated.[20] This mechanism explains the formation of acetate through weakly adsorbed acetaldehyde and bulk ethanol when free platinum sites are available:

$$C_2H_5OH + H_2O.Pt \rightarrow CHOCH_3.Pt + 2H^+ + H_2O + 2e^- \tag{21}$$
$$CHOCH_3.Pt \rightarrow CHOCH_3 + Pt \tag{25}$$
$$C_2H_5OH + OH.Pt \rightarrow CH_3COO.Pt + 4H^+ + 4e^- \tag{26}$$
$$CHOCH_3. + OH.Pt \rightarrow Pt.CH_3COO + 2H^+ + 2e^- \tag{27}$$

If we add the formation of acetic acid, water adsorption, and oxidation steps to the mechanism above, proposed electrochemical scheme takes its final form as given below;

$$C_2H_5OH + H_2O.Pt \rightarrow k_1 \rightarrow CHOCH_3.Pt + 2H^+ + H_2O + 2e^- \tag{21}$$
$$CHOCH_3.Pt \rightarrow k_2 \rightarrow CHOCH_3 + Pt \tag{25}$$
$$H_2O + Pt \rightarrow k_3 \rightarrow H20.Pt \tag{28}$$
$$H_2O.Pt \leftarrow k_4, k_{4,R} \rightarrow 0H.Pt + H^+ + e^- \tag{29}$$
$$C_2H_5OH + OH.Pt \rightarrow k_5 \rightarrow CH_3COO.Pt + 4H^+ + 4e^- \tag{26}$$
$$CHOCH_3 + OH.Pt \rightarrow k_6 \rightarrow CH_3COOH + Pt + H^+ + e^- \tag{30}$$

$$CHOCH_3. + OH.Pt \rightarrow k_7 \rightarrow Pt.CH_3COO + 2H^+ + 2e^- \quad (27)$$

In the mechanism above, Eq. (25) shows the desorption of the weakly adsorbed acetaldehyde; Eqs. (28) and (29) show the adsorption of water on platinum, which is a potential dependent (Eq. (19)), and the electrochemical oxidation of water, respectively. Eq. (30) shows the formation of soluble acetic acid through weakly adsorbed acetaldehyde. k_1, k_2, k_3, k_4, $k_{4,R}$ k_5, k_6, and k_7 in the equations above denote preexponential factors specific to electrochemical steps, and adsorption and desorption rate constants, which were explained in the previous section.

If Eq. (12) is used to find anodic faradaic current density, total anodic faradaic current can be expressed as in Eq. (31):

$$I_{faradaic} = Ir_1 + I_4 + I_5 + I_6 + I_7 \quad (31)$$

In Eq. (31), I_1 denotes anodic faradaic current by the formation of surface acetaldehyde (Eq. (21)). I_4 is the anodic faradaic current by the oxidation of surface water (Eq. (29)). I_5 is the anodic faradaic current by the formation of surface acetate through bulk ethanol (Eq. (26)). I_6 is the anodic faradaic current by the formation of soluble acetic acid through the oxidation of soluble acetaldehyde (Eq. (30)). I_7 is the anodic faradaic current by the formation of surface acetate through soluble acetaldehyde (Eq. (27)). I_1, I_4, I_5, I_6, and I_7 can be expressed in terms of Butler-Volmer equations given below in Eqs. (32)-(36) (which are similar to Eqs. (15)-(18)):

$$I_1 = n_1.F.k_1.C_{C2H5OH}(z,r,t).C_{H2O.S}(r,t).exp((1-\gamma).F.(\varepsilon(t) - \varepsilon_1^o)/(R.T)) \quad (32)$$

$$I_4 = n_4.F.[k_4.C_{H2O..S}(r,t).exp((1-\gamma).F.(\varepsilon(t) - \varepsilon_4^o)/(R.T))] \quad (33)$$

$$I_5 = n_5.F.k_5.C_{C2H5OH}(z,r,t).C_{OH..S}(r,t).exp((1-\gamma).F.(\varepsilon(t) - \varepsilon_5^o)/(R.T)) \quad (34)$$

$$I_6 = n_6.F.k_6.C_{CHOCH3}(z,r,t).C_{OH..S}(r,t).exp((1-\gamma).F.(\varepsilon(t) - \varepsilon_6^o)/(R.T)) \quad (35)$$

$$I_7 = n_7.F.k_7.C_{CHOCH3}(z,r,t).C_{OH..S}(r,t).exp((1-\gamma).F.(\varepsilon(t) - \varepsilon_7^o)/(R.T)) \quad (36)$$

In Eqs. (32) through (36), the unit of preexponentials k_1, k_5, k_6, and k_7 are $cm^5.mol^{-1}.s^{-1}$ and k_4 is cm^2/s. n_i is number of equivalence (neq/mol) specific for each faradaic current step. Electrochemical parameters to calculate faradaic currents are given in Table 2.

Table 2. Electrochemical surface reaction mechanism on layer I.

Equation no.	Electrochemical reactions	ε^o (V vs. RHE)
21	$C_2H_5OH + H_2O.Pt \rightarrow CHOCH_3.Pt + 2H^+ + H_2O + 2e-$	0.35[4−8]
29	$H_2O.Pt \leftrightarrow OH.Pt + H^+ + e^-$	0.57[27]
26	$C_2H_5OH + OH.Pt \rightarrow CH_3COO.Pt + 4H^+ + 4e-$	0.57[28]
27	$CH_3CHO + OH.Pt \rightarrow CH_3COO.Pt + 2H^+ + 2e-$	0.57[20]
30	$CHOCH_3 + OH.Pt \rightarrow CH_3COOH + Pt + H^+ + e-$	0.57[4−8]

After proper equations for diffusion and surface reaction model were set, simulation of the model was performed by using the flow chart and the parameters given in Figure 2 and Table 3. A matlab code was written to solve the partial (Equation 1) and ordinary differential equations (Eqs. (15)-(18)) using proper boundary and initial conditions (Eqs. (3), (5), and (6)) and to evaluate diffusion and faradaic currents.

Table 3. Model parameters.

Parameter	Value
Radius of disk electrode, ro (cm)	0.2
Depth of electrolyte solution, L (cm)	1×10^{-6}
Initial concentration of ethanol (mol/cm^3)	0.5
Initial concentration of active surface sites (mol/cm^2)	4.447×10^{-9}
Symmetry factor, γ	0.5
Reaction temperature, T(K)	298
Time of electro-oxidation (s)	10
Scan rate (mV/s)	100

Experimental

In order to see if the ethanol electro-oxidation model (with the proposed mechanism) can describe the real behavior, it was decided to compare the total current (diffusion plus faradaic current) with the experimental. The experiments were carried out in an air sealed glass cell, which had 3 separate compartments for the working, counter, and reference electrodes. A platinum wire was used as the counter electrode, which was separated from the working electrode with a glass compartment that has a fine porous frit at the bottom. A standard calomel electrode was used as a reference electrode. Polycrystalline platinum disk was used as a working electrode. The working electrode with a 2 mm diameter was polished with 0.1 and 0.05 μm Al_2O_3 paste and washed ultrasonically for 1 h in deionized water.

A solution of 0.5 M H_2SO_4 + 0.5 M C_2H_5OH was prepared from a high purity sulfuric acid and high purity grade ethanol (Merck Chemicals), and deionized water. The electrolyte was deaerated with ultra-high-purity helium (99.999%) before and during the experiments.

Cyclic voltammetry experiments were performed using AFCBP1 (from Pine Instruments) potentiostat-galvanostat controlled by a PC. The scan rate was 100 mV/s. The potential range was 0-1.2 V vs. RHE.

A necessary quantitative evaluation of the chemically active surface area of the catalyst was determined from the H_{upd} charge. The H_{upd} charge was found from the cathodic potential sweep (0.4-0.05 V vs. RHE) during the cyclic voltammetry in the acidic medium (Figure 3) by the charge transfer reaction (Volmer reaction):[27]

$$Pt + H^+e^- \leftrightarrow Pt - H_{ads} \tag{37}$$

After the integration of the area under the hydrogen deposition region, total charge of 0.0539 mC was obtained after subtracting the double layer contribution, the real Pt surface area Sreal = 0.0539 mC/210 μC/cm^2= 0.257 cm^2 by assuming H_{upd} monolayer adsorption charge of 210 μC/cm^2 on polycrystalline platinum. The amount of surface Pt atoms ($N_{Pt,s}$) was calculated from Faraday's law for a one-electron reaction (Eq. (37)); $N_{Pt,s}$ = 0.0539 mC/96,485 C/mol = 0.5586 nmol. Therefore, the surface density of vacant surface sites were approximated as 0.5586 nmol/0.1256 cm^2 (disk surface area), which is equal to 4.447 nmol/cm^2. If the total number of platinum active sites is divided by the real surface area (0.5586 nmol/0.257 cm^2) it gives 2.17 nmol/cm^2.[28] Roughness factor is 2.05 (Sreal/Sdisk area).

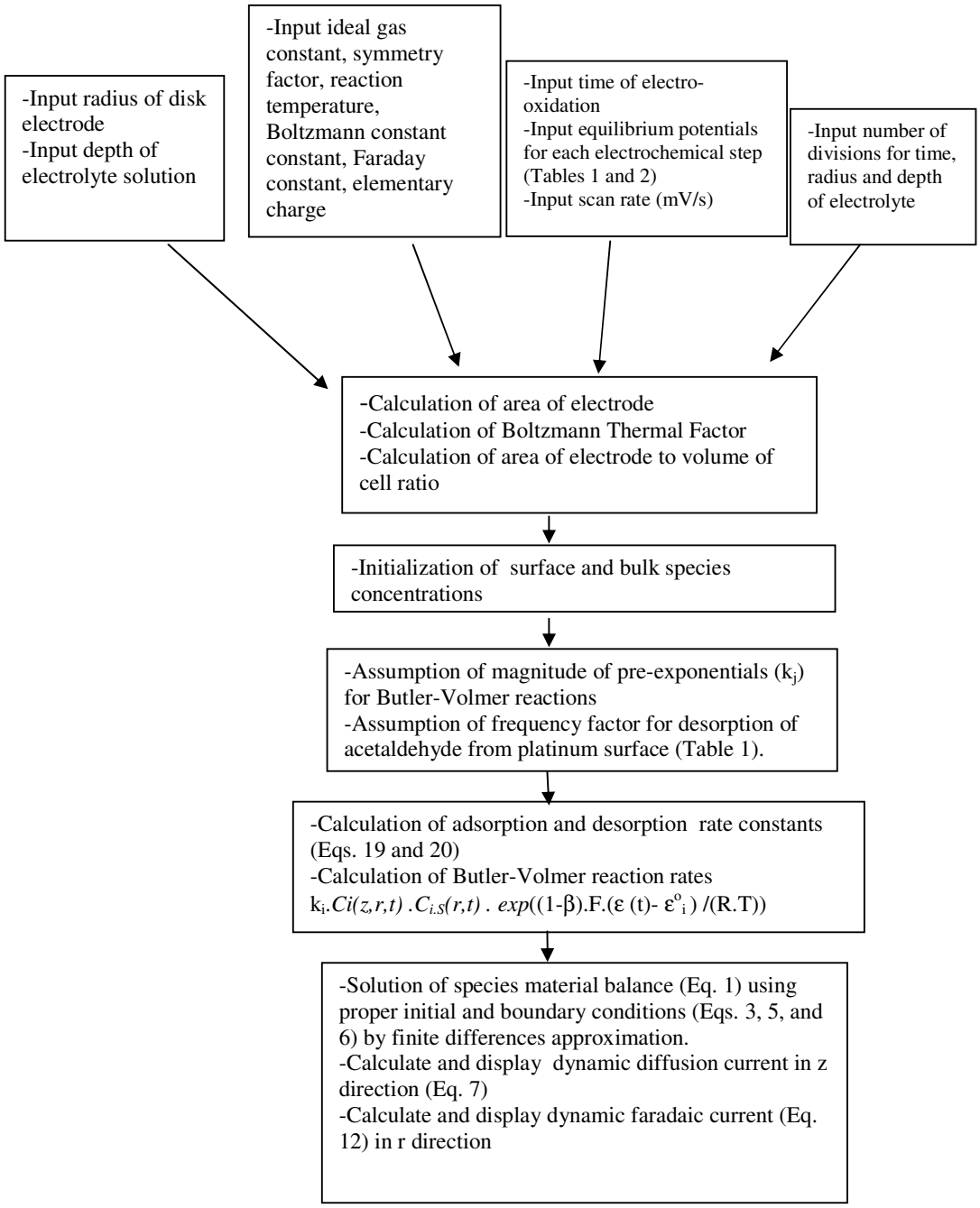

Figure 2. Flow chart of the algorithm for the ethanol electro-oxidation model.

Staircase voltammetry

Staircase voltammetry experiments were performed between 0 and 1 V vs. RHE at a scan rate of 100 mV/s. In order to see the effect of ethanol electro-oxidation, 2 kinds of staircase voltammetry experiments were performed: the first with 0.5 M H_2SO_4 electrolyte solution, and the second with 0.5 M H_2SO_4 + 0.5 M C_2H_5OH electrolyte solution. The experiments for the second electrolyte solution (0.5 M H_2SO_4 + 0.5 M C_2H_5OH) were repeated 4 times and the average current was corrected for the background current (0.5 M

H_2SO_4) (Figure 4). Staircase voltammetry was selected to analyze ethanol oxidation since we were able to compare background corrected oxidation current with the simulation in the forward scan (0-0.1 V vs. RHE) at the selected scan rate.

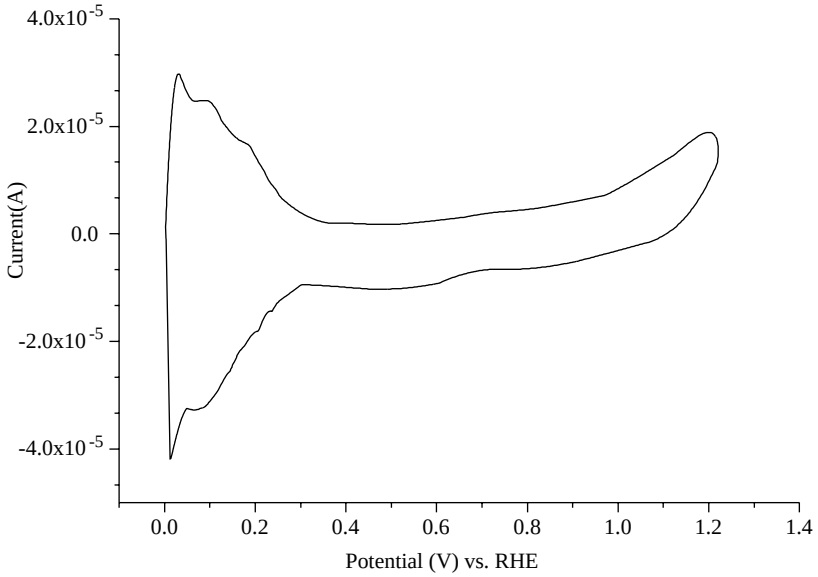

Figure 3. Cyclic voltammetry of platinum disk electrode at a scan rate of 100 mV/s in 0.5 M H_2SO_4 solution.

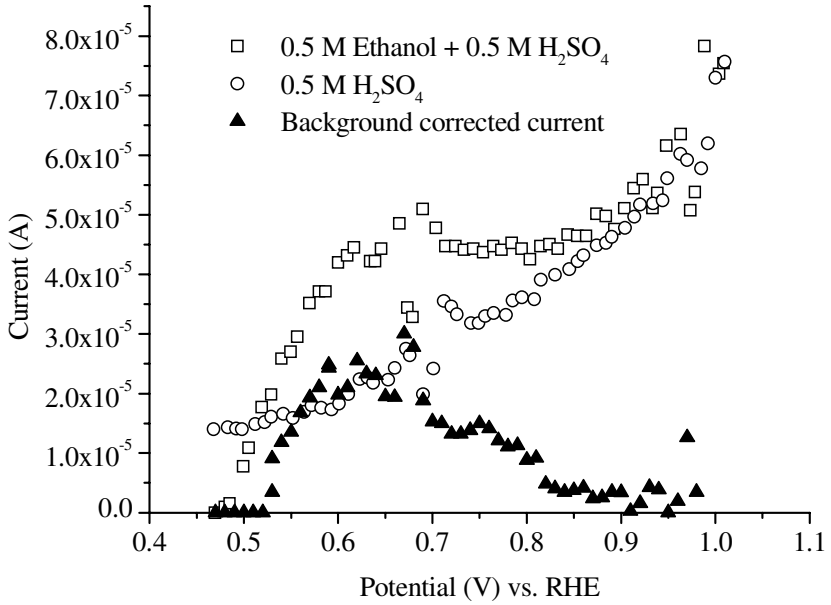

Figure 4. Background correction of ethanol electro-oxidation by staircase voltammetry.

Results and Discussion

In order to fit the ethanol electro-oxidation model to the experimental and to see the effect of preexponentials on the total faradaic current density, different magnitudes of preexponentials were selected (Figure 5). It was observed that as the rates of faradaic current steps (Eqs. (21),(29),(26),(30), and (27)) are decreased

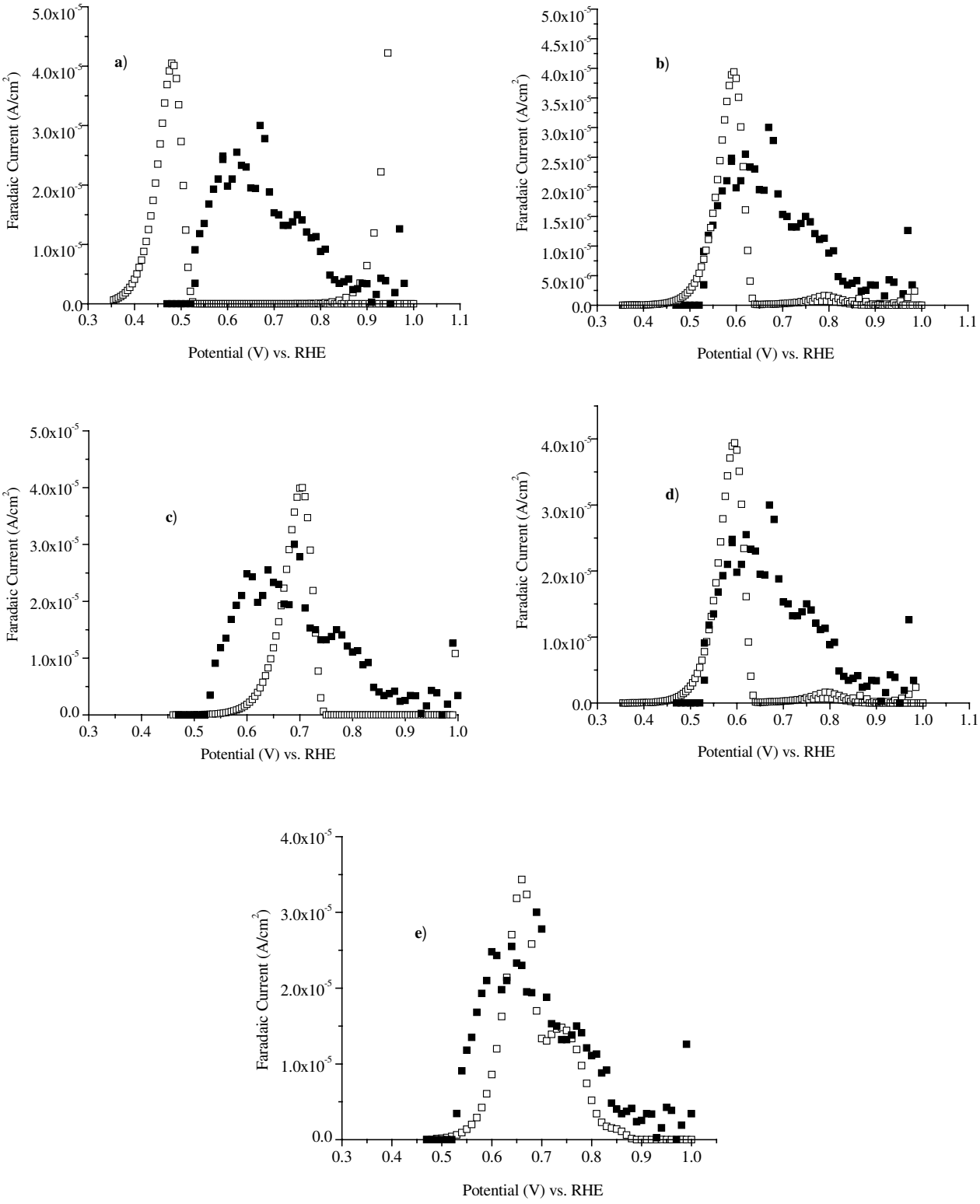

Figure 5. Comparison of the model with the experimental. Open squares represent model faradaic currents, solid squares represent experimental faradaic currents. (a) k_1, k_4, k_5, k_6, $k_7 = 1$, (b) k_1, k_4, k_5, $k_6 = 1 \times 10^{-2}$, (c) k_1, k_4, k_5, k_6, $k_7 = 1 \times 10^{-4}$, (d) $k_1 = 1 \times 10^{-2}$, k_4, k_5, k_6, $k_7 = 1$, (e) $k_1 = 1 \times 10^{-4}$, k_4, k_5, k_6, $k_7 = 1$.

by changing preexponentials the peak current shifts to more positive potentials. Another observation was the formation of a hunch around 0.75 V vs. RHE as the rates of faradaic current steps (denoted by Eqs. (17)-(20)) were increased from 1×10^{-4} to 1 $cm^5.mol^{-1}.s^{-1}$ (Figures 5c and 5e).

The formation of the hunch was mainly due to the oxidation of water since the magnitude of this faradaic current step is the highest in that potential range (Figure 8). It was decided that, when k_1 is equal to 1×10^{-4} $cm^5.mol^{-1}.s^{-1}$, k_4 is equal to 1 cm^2/s, k_5, k_6, and k_7 are equal to 1 $cm^5.mol^{-1}.s^{-1}$ in magnitude, our model can best describe the experimental data (background corrected current). The electro-oxidation model and the experimental data follow almost the same behavior when the total current densities are compared (Figure 6).

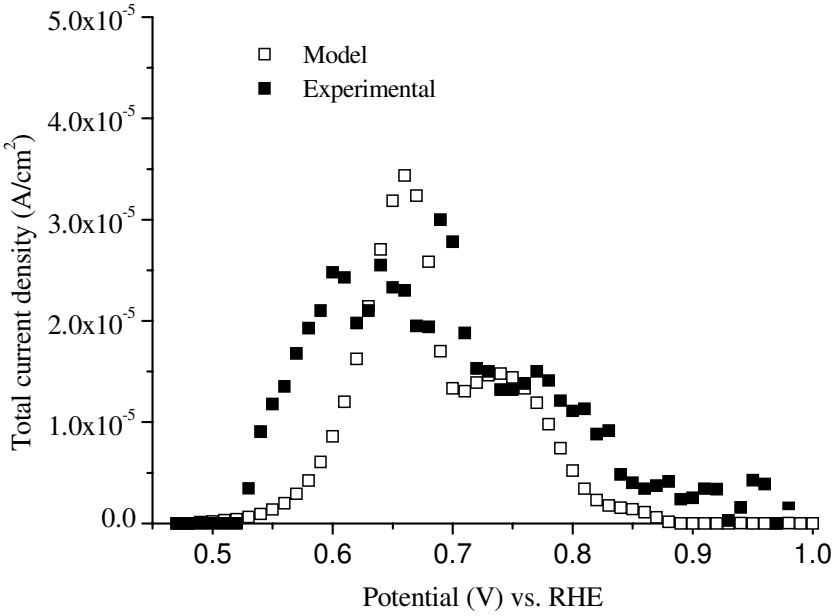

Figure 6. Comparison of the ethanol electro-oxidation model with the experimental.

The contribution of diffusion current to the total current is less than 10% and almost follows the same behavior as the faradaic current profile (Figure 7). The statistical analysis also shows that model current densities fall in the 95% confidence interval (Table 4). The total current was calculated as the summation of the maximum faradaic current in the r direction and the maximum diffusion current in the z direction. The radial diffusion current was neglected since the magnitude was very low compared to other current types with the selected model parameters.

Figure 8 shows that the formation of acetaldehyde (I_1) through the oxidation of bulk ethanol (Eq. (21)) is the rate determining the step between 0.6 and 0.75 V vs. RHE because this faradaic current step gives the highest current peak. After 0.75 V vs. RHE, the formation of surface acetate through bulk ethanol (Eq. (18)) becomes the rate-determining step (I_4). Other electrochemical steps like the formation of acetic acid and acetate through soluble acetaldehyde (Eqs. (19) and (20)) did not have an appreciable contribution to the faradaic current density profile.

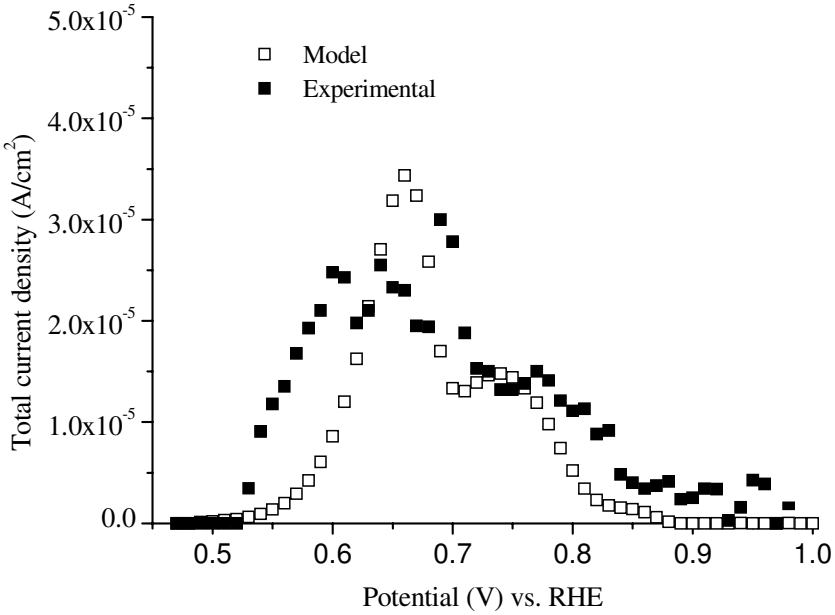

Figure 7. Comparison of faradaic current density with diffusion current density (a) Faradaic current density (b) Diffusion current density.

Table 4. Statistical analysis of the comparison of oxidation model with the experimental.

E (V)	Experimental Average Current density (A/cm^2)	Standard deviation (A/cm^2)	95% Confidence (A/cm^2)	Minimum (A/cm^2)	Maximum (A/cm^2)	Model Faradaic Current (A/cm^2)	Model Diffusion current (A/cm^2)	Model Total current (A/cm^2)
0.49	0	-	-	-	-	0	0	0
0.53	3.45×10^{-06}	8.50×10^{-07}	8.33×10^{-07}	2.62×10^{-06}	4.28×10^{-06}	1.27×10^{-07}	3.65×10^{-09}	1.30×10^{-07}
0.57	1.68×10^{-05}	1.15×10^{-06}	1.13×10^{-06}	1.56×10^{-05}	1.79×10^{-05}	6.06×10^{-07}	1.70×10^{-08}	6.23×10^{-07}
0.61	2.43×10^{-05}	2.50×10^{-06}	2.45×10^{-06}	2.18×10^{-05}	2.67×10^{-05}	2.84×10^{-06}	7.92×10^{-08}	2.92×10^{-06}
0.65	2.33×10^{-05}	1.73×10^{-06}	1.70×10^{-06}	2.16×10^{-05}	2.49×10^{-05}	1.16×10^{-05}	3.43×10^{-07}	1.20×10^{-05}
0.69	3.00×10^{-05}	2.31×10^{-06}	2.26×10^{-06}	2.77×10^{-05}	3.23×10^{-05}	3.07×10^{-05}	1.13×10^{-06}	3.19×10^{-05}
0.73	1.50×10^{-05}	2.00×10^{-06}	1.96×10^{-06}	1.30×10^{-05}	1.70×10^{-05}	1.66×10^{-05}	4.38×10^{-07}	1.70×10^{-05}
0.77	1.50×10^{-05}	1.53×10^{-06}	1.50×10^{-06}	1.35×10^{-05}	1.65×10^{-05}	1.41×10^{-05}	5.02×10^{-07}	1.46×10^{-05}
0.81	1.13×10^{-05}	1.96×10^{-06}	1.92×10^{-06}	9.36×10^{-06}	1.32×10^{-05}	1.13×10^{-05}	6.48×10^{-07}	1.19×10^{-05}
0.85	4.03×10^{-06}	2.51×10^{-06}	2.46×10^{-06}	1.57×10^{-06}	6.49×10^{-06}	2.78×10^{-06}	6.36×10^{-07}	3.41×10^{-06}
0.89	2.37×10^{-06}	1.59×10^{-06}	1.56×10^{-06}	8.04×10^{-07}	3.93×10^{-06}	7.56×10^{-07}	6.39×10^{-07}	1.40×10^{-06}
0.93	2.60×10^{-07}	4.50×10^{-07}	4.41×10^{-07}	0	7.01×10^{-07}	0	0	0
0.97	0	0	0	0	0	7.91×10^{-10}	6.43×10^{-10}	1.43×10^{-09}
1	3.42×10^{-06}	5.36×10^{-06}	5.25×10^{-06}	0	8.68×10^{-06}	0	0	0

According to the SEIRA studies of ethanol electro-oxidation on the platinum electrode (surface roughness 7) in 0.1 M $HClO_4$ + 0.1 M C_2H_5OH electrolyte solution, with increasing potential, the absorbance band at 1620-1635 cm^{-1} becomes broader and its frequency increases, and it disappears at about 0.88 V vs. RHE. This band was assigned to weakly adsorbed acetaldehyde or acetyl. When the adsorbed residues of ethanol oxidation were considered, no absorption bands were observed for acetaldehyde. This was attributed to its weaker adsorption band or small content.[20] When the coverage profiles from the simulation of the model were analyzed (Figure 9), acetaldehyde coverage starts around 0.55 V vs. RHE and reaches a constant value

around 1 V vs. RHE. This unlikely behavior of acetaldehyde, when compared with the literature, may depend on 3 reasons. First, the roughness factors differ in value (7 [20] and 2.05), and if the roughness factor is greater than 1, it is known that the behavior of rough electrodes cannot be generalized because of the experimental variables during their preparation and the change of microstructure.[29] Secondly, there is a strong anion affect on ethanol oxidation at platinum electrodes. The results show that different anions (perchlorate, sulfate, and nitrate) influence the peak current and the potential for anodic waves.[30] Thirdly, from the linear sweep voltammetry experiments, no appreciable oxidation currents were detected after background correction (Figure 4). As mentioned above, before 0.5 V vs. RHE, the oxidation current was linked to the oxidation of linearly bonded carbon monoxide through acetyl or strongly bonded acetaldehyde (Eqs. (21)-(24)).

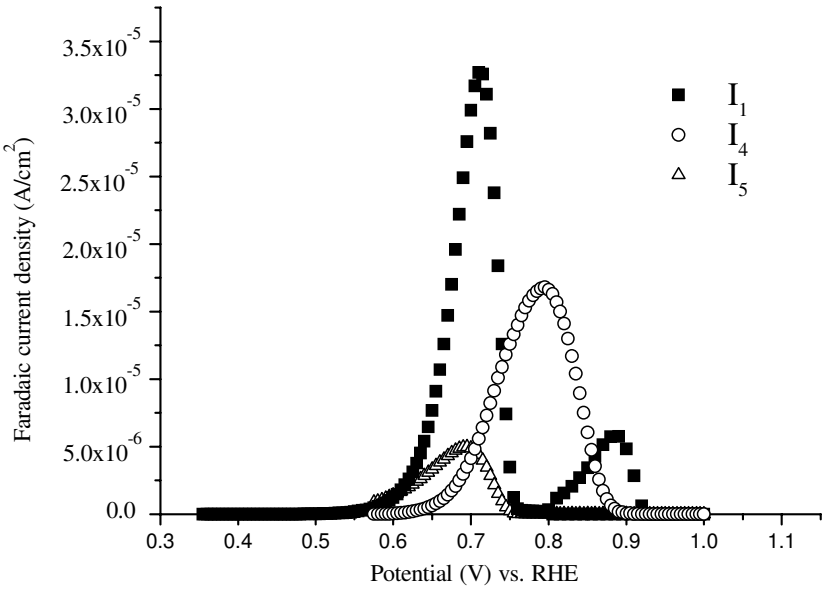

Figure 8. Faradaic current profiles from the ethanol electro-oxidation model.

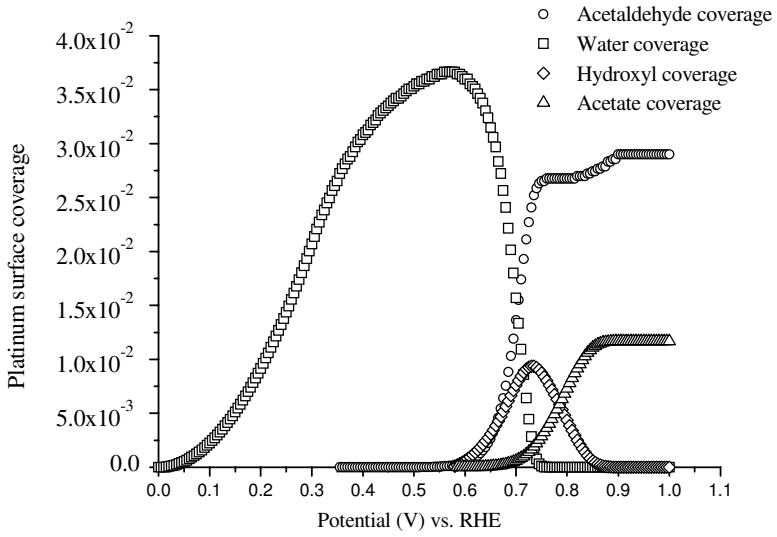

Figure 9. Surface coverage profiles from the ethanol electro-oxidation model.

Figure 9 shows the coverage profiles of the surface oxidation products with respect to the applied cell potential. After around 0.7 V vs. RHE, acetaldehyde coverage becomes the major surface species, and acetate formation starts around 0.7 V vs. RHE. The behavior of the acetaldehyde coverage matches the FTIR experiments on platinum electrodeposits polarized at 0.5 V vs. RHE in 1 M C_2H_5OH + 0.1 M HCl electrolyte solution.[21]

Conclusions

Our simple model, based on diffusion and surface reaction, can explain ethanol oxidation behavior on a platinum disk electrode. According to the model, ethanol oxidation current is determined by formation of acetaldehyde and acetate through ethanol before 0.75 V and after 0.75 V vs. RHE. Acetaldehyde is the main surface poisoning species in the potential range between 0.5 and 1 V vs. RHE. Further work will be done by adding different ethanol electro-oxidation steps to the proposed mechanism, like the surface CO formation step through strongly adsorbed acetaldehyde. It is thought that, with the model developed in this study, we can monitor the surface species concentrations and the current-time profiles of any proposed oxidation mechanism, and test the existence of the mechanism by comparing the model with voltammetric experiments.

Acknowledgments

Special thanks to TÜBİTAK for the financial support.

References

1. W. Vielstich, **"In fuel cells: Modern processes for the electrochemical production of energy"** eds. D.J.G. Ives, Wiley-Interscience, New York, 1970.
2. W. Zhou, S. Zhou, S. Song, W. Li, G. Sun, P. Tsiakaras and Q. Xin, **Applied Catalysis B: Environmental 46**, 273-285 (2003).
3. A.J. Bard and L.R. Faulkner, **"Electrochemical Methods: Fundamentals and Applications"**, 2^{nd} ed. John Wiley & Sons, 2001.
4. F. Vigier, C. Countanceau, F. Hahn, E.M. Belgsir and C. Lamy, **Journal of Electroanalytical Chemistry 563**, 81-89 (2004).
5. J.P.I. Souza, F.J.B. Rabelo, I.R. De Morales and F.C. Nort, **Journal of Electroanalytical Chemistry 420**, 17 (1997).
6. R. Ionniello, V.M. Schmidt , J.L. Rodriquez and E. Pastor, **Journal of Electroanalytical Chemistry 471**, 167 (1999).
7. N. Fujiwara, K.A. Friedrich and U. Stimming, **Journal of Electroanalytical Chemistry 472**, 120 (1999).
8. H. Hitmi, E.M. Belgsir, J.M. Leger, C. Lamy and R.O. Lezna, **Electrochimica Acta 39**, 407 (1994).
9. A. Constantinides and N. Mostoufi, **"Numerical Methods for Chemical Engineers with MATLAB Applications"**, Prentice-Hall, 1999.
10. K. Okamoto, N. Hirota and M. Terazima, **Journal of Physical Chemistry A**, **102**, 3447-3454 (1998).

11. Y. Yu and G.H. Gao, **Fluid Phase Equilibria 179**, 165-179 (2001).
12. M.L. Rosinberg, J.L. Lebowitz and L. Blum, Journal of Statistical Physics 44, 153 (1986).
13. D.A. Huckaby and L. Blum, **Journal of Chemical Physics 92**, 2646 (1990).
14. L. Blum and D.A. Huckaby, **Journal of Chemical Physics 94**, 6887 (1991).
15. D.A. Huckaby, M.D. Legault and L. Blum, Journal of Chemical Physics 109, 3600 (1998).
16. L. Blum and D. Henderson, Journal of Chemical Physics 74, 1902 (1981).
17. L. Blum, F. Vericat and W.R. Fawcett, Journal of Chemical Physics 96, 3039 (1992).
18. L. Blum and W.R. Fawcett, **Journal of Chemical Physics 97**, 7185 (1993).
19. Y. Shingaya and M. Ito, **Surface Science 386**, 34-47 (1997).
20. M.H. Shao and R.R. Adzic, **Electrochimica Acta 50**, 2415-2422 (2005).
21. G.A. Camara, R.B. Lima and T. Iwasita, **Journal of Electroanalytical Chemistry**, **585**, 128 (2005).
22. M. Bhattacharya, W.G. Devi and P.S. Mazumdar, **Applied Surface Science 218**, 1-6 (2003).
23. O. Deutschmann, R. Schmidt, F. Behrendt and J. Warnatz, **Twenty-Sixth International Symposium on Combustion**, 1747-1754 (1996).
24. O. Deutschmann, F. Behrendt, J. Warnatz, C.T. Goralski and L.D. Schmidt, **Catalysis Today**, **21**, 461 (1994).
25. M.A. Natal-Santiago, J.M. Hill and J.A. Dumesic, **Journal of Molecular Catalysis A: Chemical, 140**, 199-214 (1999).
26. A.B. Anderson and T.V. Albu, **Journal of The Electrochemical Society**, **147**, 4229-4238 (2000).
27. K. Kinoshita and P. Stonehart, **"Modern Aspects of Electrochemistry"** eds. J.O'M. Bockris, and B.E. Conway, Plenum Press, New York, 1986.
28. A. Wieckowski, W. Chrzanowski and G.Q. Lu, **Journal of Physical Chemistry B 104**, 5566-5572 (2000).
29. H. Hoster, T. Iwasita, H. Baumgartner and W. Vielstich, **Journal of the Electrochemical Society 148**, A496-A501, (2001).
30. K.D. Snell and A.G. Keenan, **Electrochimica Acta**, **27**, 1683-1696 (1982).